Exact relativistic time evolution for a step potential barrier

Jorge Villavicencio†

Abstract. We derive an exact analytic solution to a Klein-Gordon equation for a step potential barrier with cutoff plane wave initial conditions, in order to explore wave evolution in a classical forbidden region. We find that the relativistic solution rapidly evanesces within a depth $2x_p$ inside the potential, where x_p is the penetration length of the stationary solution. Beyond the characteristic distance $2x_p$, a Sommerfeld-type precursor travels along the potential at the speed of light, c. However, no spatial propagation of a main wavefront along the structure is observed. We also find a non-causal time evolution of the wavefront peak. The effect is only an apparent violation of Einstein causality.

† Facultad de Ciencias, Universidad Autónoma de Baja California
Apartado Postal 1880, Ensenada, Baja California, México.

1. Introduction

Since the early beginnings of quantum mechanics, the problem of particle propagation in classical forbidden regions has been the subject of both theoretical and experimental investigations. Over the years, several non-relativistic approaches based in cutoff wave initial conditions have been introduced in the literature in order to investigate the time-dependent features of wave evolution in evanescent media. Some of these theoretical models [1, 2, 3, 4, 5] were inspired in the pioneering work of Sommerfeld and Brillouin [6, 7], while others [9, 10, 11, 12] were based in the seminal work of Moshinsky [13, 14], who a few decades ago started a fundamental discussion on the non-relativistic and relativistic transient effects. These models represent important steps towards the clarification of the dynamics in classical forbidden regions, and a renewed motivation to explore this problem has been recently stimulated by the issue of superluminal velocities in photon [15, 16] and microwave [17, 18] tunneling. Hence, it is clear that a full relativistic approach to describe the wave evolution in evanescent media is needed. Nevertheless, this has become a complex problem due to the lack of exact analytical solutions to relativistic wave equations with appropriate initial conditions. Among the few works in the field [19, 4, 5], Deutch and Low [19] have provided a lucid description of barrier penetration of an initial state given by a cutoff Gaussian wavepacket, based on a one-dimensional Klein-Gordon equation. Although no exact relativistic solutions were obtained, the issues of Einstein causality and superluminal phenomena were rigorously discussed using approximate solutions.

In this paper we consider a model based on the Klein-Gordon equation, as in the work of Deutch and Low [19], for a potential step barrier and cutoff plane wave initial conditions. We obtain an exact analytic solution to the problem along the potential region and study the main features of wave evolution, in particular the regime of transient effects at early times.

The paper is organized as follows. In section 2 we discuss the shutter problem, and present the analytical derivation for the solution to a relativistic wave equation for a step potential barrier. Section 3 deals with a numerical example for the solution along the internal region of the potential, and the results are discussed in section 4. Finally, in section 5 we present the summary and conclusions.

2. The relativistic shutter problem

To investigate the time evolution of cutoff plane wave in a classical forbidden region, let us consider a classical field ψ_r^s satisfying a one-dimensional Klein-Gordon equation with a variable potential $V(x)$, as in the model of Deutch and Low [19],

$$\frac{\partial^2}{\partial x^2}\psi_r^s(x,k_r,t) = \frac{1}{c^2}\frac{\partial^2}{\partial t^2}\psi_r^s(x,k_r,t) + V_0(x)\psi_r^s(x,k_r,t). \tag{1}$$

In our case, $V_0(x)$ is given by a step potential barrier,

$$V_0(x) = \begin{cases} \mu_0^2, & x \geq 0, \\ 0, & x < 0, \end{cases} \tag{2}$$

where $\mu_0 = (m_0 c/\hbar)$, and the initial condition at $t = 0$ corresponds to a plane wave shutter [11] (see figure 1), given by,

$$\psi_r(x, t=0) = \begin{cases} e^{ik_r x} - e^{-ik_r x}, & x \leq 0, \\ 0, & x > 0. \end{cases} \tag{3}$$

The simplicity of our quasi-monochromatic initial state (3), allows a closed analytical solution of the problem. It differs from that of reference [19], where a cutoff Gaussian wavepacket initial condition was considered. Note that condition (3) comes from the fact that for $t < 0$, the solution for the left side of the shutter [20] is given by $\psi_r(x,k_r,t) = \exp[ik_r(x-ct)] - \exp[-ik_r(x+ct)]$, for $x < 0$, and zero for $x > 0$.

To obtain the solution for $x > 0$ and $t > 0$, we shall proceed along the same lines as in our recent work [11]. We begin by Laplace transforming the equation (1) using the standard definition

$$\overline{\psi}(x,k_r,s) = \int_0^\infty \psi(x,k_r,t)e^{-st}dt, \tag{4}$$

with the initial condition given by equation (3). As a consequence, one gets a pair of differential equations corresponding to the regions $x > 0$ and $x < 0$. In order to obtain the transmitted wave function, one must consider the matching conditions for the wave function and its derivative at $x = 0$. The Laplace transformed solution reads,

$$\overline{\psi}_r^s(x,s) = \frac{2E}{i\,(s+iE)\,(s+p)}e^{-px/c}, \tag{5}$$

where $p = (s^2 + \mu_0^2 c^2)^{1/2}$, and $E = k_r = (E_r/\hbar c)$ corresponds to the relativistic energy E_r given in reciprocal units of length.

The time dependent solution for $x > 0$ is readily obtained by performing the inverse Laplace transform of equation (5) using the Bromwich integral formula,

$$\psi_r^s(x,t) = \frac{1}{2\pi i}\int_{\gamma'-i\infty}^{\gamma'+i\infty} \overline{\psi}_r^s(x,s)e^{st}ds, \tag{6}$$

where the integration path is taken along a straight line $s = \gamma'$ parallel to the imaginary axis in the complex $s-$plane. The real parameter γ' can be chosen arbitrarily as long as all singularities remain to the left-hand side of $s = \gamma'$.

The integral (6) expressed in this form, is difficult to manipulate since the integrand (5) has branch points at $s = \pm i\mu_0 c$. To surmount this difficulty, let us introduce the change of variable, $-iu = (s+p)/\mu_0 c$, which allows to eliminate the branch points. Thus, $p = i\mu_0 c(u^{-1} - u)/2$, and as a consequence, the Bromwich integral may be written as,

$$\psi(x,t) = \frac{1}{2\pi i}\int_{i\gamma-\infty}^{i\gamma+\infty} F(u)du, \tag{7}$$

where the new integrand $F(u)$ is given by,

$$\begin{aligned} F(u) = \quad & \frac{2E}{\mu_0}\frac{(1-u^2)}{u^2(u^2 - 2Eu/\mu_0 + 1)} \\ & \times \exp\{i\mu_0[u(x-ct) - u^{-1}(x+ct)]/2\}. \end{aligned} \tag{8}$$

Note that the branch points go into an essential singularity at $u = 0$ and two simple poles $u_\pm = (E \pm iq)/\mu_0$, where we defined $q = ({\mu_0}^2 - E^2)^{1/2}$. The integration in equation (7) is performed along a straight line L parallel to the real axis cutting the positive imaginary axis at $i\gamma$. We proceed to evaluate the above integral by considering a closed Bromwich integration contour (see figure 2), and Cauchy's residue theorem. For $x > ct$ we close the integration path L from above, by a large semicircle Γ_1 of radius R, forming a closed contour C_1. The contribution along Γ_2 vanishes as $R \to \infty$, and since there are no poles enclosed inside C_1, $\psi(x,t) = 0$ for $x > ct$. For the case $x < ct$, we close the integration path from below with a large semicircle Γ_2. The closed contour C_2 contains three small circles $C_{0,}$ C_+ and C_- enclosing the essential singularity at $u = 0$ and the simple poles at u_+ and u_-, respectively. Hence by using Cauchy's theorem, it follows that,

$$\frac{1}{2\pi i}\left[\int_{i\gamma-\infty}^{i\gamma+\infty} - \int_{\Gamma_2} + \int_{C_0} + \int_{C_+} + \int_{C_-}\right] F(u)du = 0. \tag{9}$$

The integrals corresponding to the contours C_+ C_- can be easily evaluated, and yield the exponential contributions to (9), namely,

$$\frac{1}{2\pi i}\int_{C_\pm} F(u)du = k_\pm e^{(\mp qx - iEct)}, \tag{10}$$

where we defined $k_\pm = 2E/(E \pm iq)$.

The contour integration for C_0 requires a more elaborate calculation, since involves an essential singularity at $u = 0$. For this case, we introduce the change of variable given by $\omega = -iu\xi^{-1}$, thus the integral now becomes

$$\int_{C_0} F(u)du = \int_{C_0'} \frac{2E}{i\mu_0\xi^3} \frac{(1+\omega^2\xi^2)exp[\eta(\omega-\omega^{-1})/2]}{\omega^2(\omega-\omega_+)(\omega-\omega_-)} d\omega, \tag{11}$$

where $\omega_\pm = (E \pm iq)/i\mu_0\xi$. To carry out the integration, first let us separate the integrand into partial fractions, and substitute the well known formula for the Bessel generating function,

$$e^{\eta(\omega-\omega^{-1})/2} = \sum_{n=0}^{\infty} \omega^n J_n(\eta) + \sum_{n=1}^{\infty} (-1)^n \omega^{-n} J_n(\eta) \tag{12}$$

and the series expansion,

$$(\omega_\pm - \omega)^{-1} = (\omega_\pm)^{-1} \sum_{n=0}^{\infty} (\omega/\omega_\pm)^n J_n(\eta). \tag{13}$$

The resulting integrals can be evaluated by means of the residue theorem. For the case of an essential singularity, the residue may be determined by computing explicitly the coefficient corresponding to ω^{-1} from the series expansion and their products. In that case, equation (11) becomes,

$$\begin{aligned} \frac{1}{2\pi i}\int_{C_0} F(u)du = \quad & \left[\frac{2iE}{\mu_0\xi} J_1(\eta) - k_+ \sum_{n=0}^{\infty} (-1)^n \frac{J_n(\eta)}{(\omega_+)^n} \right. \\ & \left. -k_- \sum_{n=0}^{\infty} (-1)^n \frac{J_n(\eta)}{(\omega_-)^n} \right]. \end{aligned} \tag{14}$$

Finally, substituting the results given by equations (14) and (10) into equation (9), the solution for the internal region is,

$$\psi_r^s(x,t) = \begin{cases} \psi_+(q) + \psi_-(q), & t > x/c \\ 0, & t < x/c, \end{cases} \tag{15}$$

with $\psi_\pm(q)$ defined as,

$$\begin{aligned} \psi_\pm(q) = \quad & k_\pm \left[e^{(\mp qx - iEct)} + \frac{iz_\pm}{2\xi} J_1(\eta) \right. \\ & \left. - \sum_{n=0}^{\infty} (\xi/iz_\pm)^n J_n(\eta) \right]. \end{aligned} \tag{16}$$

In the above expression, $J_n(\eta)$ stands for the Bessel function of order n. The other parameters are defined as: $\xi = [(ct+x)/(ct-x)]^{1/2}$, $\eta = \mu_0(c^2t^2 - x^2)^{1/2}$ and $z_\pm = (E \pm iq)/\mu_0$. From equation (15) we see that the solution obeys Einstein

causality, i.e. no propagation faster than the speed of light, c, is detected along the barrier region. In other words, an observer located at an arbitrary position x_0 inside the barrier must wait a time $t = (x_0/c)$ before detecting the arrival of the signal.

For the sake of completeness, let us now consider the asymptotic behavior of $\psi_r^s(x,t)$ for the cases $\mu_0 \to 0$, $t \to \infty$ and $x \to ct$. From the solution we have just discussed, one may recover the free propagation solution in the limit $\mu_0 \to 0$. This corresponds to let the variables $\eta \to 0$, $q \to iE$. To illustrate the limit process in equation (15), let us rewrite the solution by using equation (12), namely,

$$\begin{aligned}\psi_r^s(x,t) = \quad & k_- \left[e^{(qx-iEct)} - J_0(\eta) \right. \\ & \left. - \sum_{n=1}^{\infty} (\xi/iz_-)^n J_n(\eta) \right] \\ & + k_+ \left[\sum_{n=2}^{\infty} (z_+/i\xi)^n J_n(\eta) \right]. \end{aligned} \tag{17}$$

As $\mu_0 \to 0$, the variable $J_0(\eta) \to 1$, and since $(z_-)^{-1} \to 0$ the first series on the right hand-side clearly vanishes. It can be shown that the second series also vanishes, by replacing the Bessel functions by their asymptotic values for small values of the argument η,

$$J_n(\eta) \simeq 2^{-n}\eta^n/n!. \tag{18}$$

Therefore, one obtains the solution for the free propagation case,

$$\psi_r^s(x,t) \to \begin{cases} e^{ik_r(x-ct)} - 1, & t > x/c, \\ 0, & t < x/c. \end{cases} \tag{19}$$

Note that the free case solution rises from zero only after a time $t = (x/c)$ fulfilling relativistic causality, and then oscillates periodically thereafter.

In the case of the long-time limit ($t \to \infty$), we have $\xi \to 1$ and $\eta \to \infty$. From the asymptotic expansion of $J_n(\eta)$ for large values of the argument η,

$$J_n(\eta) \simeq \frac{1}{(\pi\eta/2)^{1/2}} cos[\eta - \frac{1}{4}(2n+1)\pi], \tag{20}$$

and therefore $J_n(\eta) \to 0$. One can see from equation (16) that the series in $\psi_+(q)$ vanishes. On the other hand, if we rewrite $\psi_-(q)$ by means of equation (12), the exponential term is canceled and the remaining series vanishes. Consequently, $\psi_r^s(x,t)$ goes into the stationary solution $\phi_r^s(x,t)$ given by,

$$\phi_r^s(x,t) = k_+ e^{-qx} e^{-iEct}. \tag{21}$$

The asymptotic behavior near the relativistic cutoff, is obtained when $x \to ct$ in equation (15). In this case we have $\eta \to 0$, which allows us to substitute the asymptotic expansion (18) in $\psi_+(q)$ (equation (16)). Thus, the series of equation (16) goes into an exponential function, which cancels exactly with the exponential term, and as a result the solution $\psi_+(q)$ goes like $iEJ_1(\eta)/\mu_0\xi$. From similar considerations on $\psi_-(q)$, an identical expression is obtained and the approximate behavior of $\psi_r^s(x,t)$ near the cutoff is given by,

$$\psi_r^s(x,t) \approx \frac{2iE}{\mu_0\xi} J_1(\eta), \tag{22}$$

where for exactly the value $x = ct$, the above expression goes to zero fulfilling relativistic causality.

3. Examples

In order to exemplify the evolution of the solution given by equation (15) along the evanescent region, we decided to study the properties of $|\psi_r^s(x,t)|^2$ as a function of time t and the position x. The parameters for the system considered in all the cases for the present study are: barrier height $\mu_0 = 1.542\ nm^{-1}$, incidence energy $E_r = 10.0\ eV$ ($E = 5.064 \times 10^{-2}\ nm^{-1}$).

The first case corresponds to the spatial evolution of $|\psi_r^s(x,t)|^2$ along the dispersive region. In figure 3 we show at early times the birth of the main wavefront as a function of the position, for increasing values of time: $t_1 = .001\ fs$, $t_2 = .0035\ fs$ and $t_3 = .0075\ fs$. The solution rises as time goes on, and at t_3, $|\psi_r^s(x,t)|^2$ has already crossed over the stationary solution $|\phi_r^s(x,t)|^2$ (dashed line). The inset of figure 3 shows the crossover of $|\psi_r^s(x,t)|^2$ at later time $t_4 = .012\ fs$. This behavior is relevant since it indicates that the relativistic solution fluctuates around $|\phi_r^s(x,t)|^2$, before reaching its asymptotic regime. At the inset, we can also observe how the solution evanesces within a finite depth given approximately by $2x_p = 1.317\ nm$, where $x_p = (1/q)$ is the *penetration length* of the stationary solution $|\phi_r^s(x,t)| = |k_+|e^{-qx}$ (equation (21)). We find that beyond $2x_p$ the solution exhibits a small maxima, corresponding to the birth of a forerunner. In figure 4 we depict the spatial evolution of $|\psi_r^s(x,t)|^2$ (solid line) for a fixed value of $t = 0.05\ fs$. As can be seen in this example, the main part of the wave rapidly evanesces in the potential region for small values of the position. However, from approximately $2x_p$ onwards, the solution exhibits an oscillatory behavior before reaching the relativistic cutoff at $x = 15.0\ nm$, corresponding to the earliest arrival of the signal at a point located within the potential. The stationary solution $|\phi_r^s(x,t)|^2$ (dashed line) is also included for comparison. It is interesting to note the similarity of the oscillatory structure in figure 4, to the well known Sommerfeld precursor [8, 21], which is one of the essential features of wave propagation in dispersive media. Despite the fact that Sommerfeld's approach is quite different from ours, the similarities go beyond the numerical results. For instance, their asymptotic analysis showed that the wave function is governed by a first order Bessel function near the relativistic cutoff. Our analysis reproduces such behavior, which is given by equation (22). For comparison, the value of the Bessel function $J_1(\eta)$ modulated by the prefactor $2iE/\mu_0\xi$, is also included in figure 4 (dotted line). Note that if we define the frequency of the oscillations of the precursor in terms of the distance between successive zeros of $J_1(\eta)$, one sees from the definition of the argument η that the value of the frequency depends only on the position x and the potential μ_0 that characterizes the medium i.e. the precursor frequency is independent of the incidence energy.

In figure 5 we show $|\psi_r^s(x,t)|^2$ (solid line) as a function of the position x, at a subsequent time $t = 0.3\ fs$. We can see that the solution reaches its stationary value $|\phi_r^s(x,t)|^2$ (dashed line) for small values of x; nevertheless, near the relativistic cutoff at $x = 90.0\ nm$, the precursor exhibits a rich oscillatory structure. The inset of figure 5 illustrates the forerunner near the cutoff, and shows that the asymptotic behavior is dictated by the Bessel function of equation (22) (dotted line).

Up to here we have illustrated the spatial behavior of $|\psi_r^s(x,t)|^2$, and some interesting features of the time evolution. In order to fully explore the relevant features of the time evolution, in figure 6 we plot $|\psi_r^s(x,t)|^2$ as a function of time at different

positions: $x_1 = 0.4\ nm$, $x_2 = 0.6\ nm$ and $x_3 = 0.8\ nm$. For all the curves depicted, as soon as $t > (x/c)$ the solution is different from zero along the internal region, fulfilling relativistic causality. As can be seen, the solution rises from zero at $t = (x/c)$ and grows monotonically towards a maximum value, from which it starts to oscillate thereafter, forming a pattern very similar to the diffraction in time phenomenon [13]. The concept of diffraction in time was originally introduced by Moshinsky [13] while discussing the shutter problem for the free particle Schrödinger equation. He observed a time-dependent oscillatory regime of the probability density near the semiclassical wavefront that he named diffraction in time, in analogy to the well known Fresnel optical diffraction. It is interesting to note the resemblance of the oscillatory pattern in figure 6, to the diffraction in time phenomenon observed in the free propagation case [11]. Moreover, in the low-energy regime ($\mu_0/E \gg 1$) the solution (15) can be rewritten in a more concise form by using equation (12), namely,

$$\Psi_r^s(x,t) \approx 2(E/V)\left[U_3(i\eta/\xi,\eta) - U_1(i\eta/\xi,\eta)\right], \tag{23}$$

where U_1 and U_3 are the Lommel functions of two variables [23], widely used in connection with optical diffraction [24]. The resemblance to diffraction phenomena suggests that there exists a more profound link; however, the physical implications of the striking mathematical similarities found above deserves further study.

It is important to mention that the transient effect depicted in figure 6 is observed in the low-energy regime i.e. $(\mu_0/E) \gg 1$; this condition is satisfied in the present example, where the effect was observed for values of the ratio $(\mu_0/E) \simeq 30$**.** Moreover, we only observed the phenomenon in the regime of small values of the position x where the solution decays in the potential region i.e. $x < 2x_p$. From values greater than $x \simeq 2x_p$ the solution enters into a different oscillatory regime, and the diffraction-type pattern begins to disappear. In figure 7 we illustrate the inhibition of the diffraction-type pattern for a fixed value of the position $x = 3.0\ nm$. Clearly, it fades out and is replaced by a series of oscillations, which register the fast crossing of the precursor at $x = 3.0\ nm$, and the remaining forerunners.

There is another interesting feature in the time evolution of $|\psi_r^s(x,t)|^2$ that can be appreciated in figure 8, in which we plot $|\psi_r^s(x,t)|^2$ as a function of time in the main peak region. Surprisingly, the maximum peak of the wave appears on $x = 0.5$ nm (dotted line) earlier than the peak at $x = 0.3$ nm (dashed line) and $x = 0.1$ nm (solid line). This relative *time shift* of the wave peak is an apparent violation of relativistic causality, and can be interpreted as a non-causal behavior. This comes from the fact that we are comparing the maximum wave peak at different positions. However, we observe that the wavefront always fulfills Einstein causality, and no signal travels faster than c in the dispersive region. Therefore, the observed shift of the main peak may be interpreted as a reshaping of the wave and not as a genuine violation of relativity.

It is interesting to mention that we have observed a similar non-causal behavior in the probability density along a classical forbidden region of a rectangular potential barrier, within a non-relativistic framework. Moreover, some authors have also reported non-causal phenomena in electromagnetic evanescent modes [18].

4. Discussion

The possibility of describing the wave evolution from the transient to the stationary regime, offers a clear advantage over the asymptotic methods of solution available in the literature, for which the short and intermediate transient regimes are inaccessible.

In what follows, we shall discuss the new features in the dynamical process of evanescent waves observed in the previous section.

The buildup of $|\psi_r^s|^2$ exhibits a very interesting behavior; the solution instead of just grow monotonically towards the stationary solution $|\phi_r^s|^2$, fluctuates around such value before reaching the asymptotic regime, as it is shown by the series of curves of $|\psi_r^s|^2$ versus x at different times (see figure 3). The effect of these fluctuations in a plot of $|\psi_r^s|^2$ versus t (x fixed) is manifested as a series of oscillations similar to a diffraction in time pattern, see figure 6. The inset of figure 3 shows that beyond a certain distance, an interesting structure of the wave appears; this is the birth of the Sommerfeld-type forerunner which travels along the potential region, as illustrated in figures 4 and 5; the head of this signal propagates at the speed of light and can reproduced by the first order Bessel function $J_1(\eta)$ (dotted line). The birth of the forerunner is an important event since its propagation at longer times becomes the dominant process; this is also the case in the context of different relativistic and non-relativistic approaches [4, 5], where the characterization of the forerunners has been recently emphasized.

At early times and for small values of the position, the main front of the wave decays exponentially along the potential. As time goes on, the dynamics is dominated by the propagation of the forerunners since the main front rapidly reaches its asymptotic value without propagation. Thus, one may speak of two regimes, which as discussed in the previous section, are characterized by $2x_p$ where x_p is the penetration length. If we choose a position $x > 2x_p$ and wait for the main wavefront, instead of detecting its arrival we would only register the fast crossing of the precursor (see figure 7). The absence of main wavefront propagation in the evanescent region is in agreement with a series of works [9, 25, 26, 27], which have questioned the existence of semiclassical wavefront propagation proposed by Stevens [1] and supported by Moretti [2, 3].

Another important result of this work is the non-causal peakshift exhibited in figure 8. The non-causal behavior observed here is a consequence of the reshaping of the wave; reshaping effects have also been observed in the context of wavepacket evolution within both relativistic [19] and non-relativistic [22] approaches. The role of this effects and the issue of non-causal behavior has been recently discussed by Deutch and Low [19] for the case of Gaussian wavepacket evolution in the transmitted region of a potential barrier, based on approximate solutions to the Klein-Gordon equation. Although the barrier and the step potential are different systems, both exhibit an evanescent region; hence, we believe that the non-causal behavior observed in reference [19] could be related to a reshaping process occurring inside the barrier, similar to the reshaping observed in the step discussed in our model. However, in order to investigate such a reshaping inside the barrier, the solution of the Klein-Gordon equation is required for the internal region. In this respect, the analytical techniques used in this work may provide a suitable method of solution to tackle this fundamental problem; nevertheless, this not an easy task since the extension of our model to the case of a barrier of finite width involves more complicated analytical properties of the solution due to the presence of resonances.

5. Summary and conclusions

We have derived an exact analytical solution to a Klein-Gordon equation for a step potential barrier, using a cutoff plane wave initial condition. To our knowledge, this is

the first model which allows a closed solution for the description of relativistic transient effects in a classical forbidden region.

The main features of the spatial and time evolution along the evanescent region can be summarized in the following points: (i) We found a regime where the solution is exponentially suppressed and thus, decays as a function of x along the potential. This main part of the wave does not propagate along the structure. The regime is characterized by a region extending from $x = 0$ to $x \approx 2x_p$, where $x_p = (1/q)$ is the penetration length of the stationary solution (21). However, from $x \approx 2x_p$ onwards, the solution exhibits an oscillating pattern near the relativistic cutoff, traveling at the speed of light, c which can be identified as a Sommerfeld-type precursor. Also, within the finite depth $2x_p$, we found in the low-energy situation that the time evolution of $|\psi_r^s(x,t)|^2$, exhibits a transient effect similar to the diffraction in time phenomenon [13]. (ii) We showed that along the internal region, there exists a time shift associated to the main peak of the wave function, that can be interpreted as a non-causal behavior along the classical forbidden region. This of course is only an apparent violation of relativistic causality, since in our model the wavefront satisfy always Einstein causality i. e. no signal travels faster than the speed of light.

The relevance of these results, comes from the fact that our findings may be of interest to elucidate on the problem of wave propagation in finite width potentials.

Acknowledgments

I would like to thank Gastón Garcia-Calderón and Alberto Rubio, who suggested the shutter model approach to solve this problem. I am indebted to them for encouragement and valuable discussions. I would like to thank also Marcos Moshinsky for fruitful discussions on the shutter problem. Useful discussions with Roberto Romo are gratefully acknowledged. This work was supported financially by Conacyt-México under Contract No. 431100-5-32082E.

References

[1] Stevens K W H *1983 J. Phys.* C*: Solid State Phys.* **16** 3649.
[2] Moretti P 1992 *Phys. Rev.* A **46** 1233.
[3] ——1992 *Physica Scripta* **45** 18.
[4] Büttiker M and Thomas H 1998 *Superl. Microstruc.* **23** 781.
[5] Muga J G and Büttiker M 2000 *Phys. Rev.* A **62** *023808.*
[6] Sommerfeld A 1914 *Ann. Phys.* **44** 177.
[7] Brillouin L 1914 *Ann. Phys.* **44** 203.
[8] ——1960 *Wave Propagation and Group Velocity* (Academic Press, New York) p. 74.
[9] Brouard S and Muga J G 1996 *Phys. Rev.* A **54** 3055.
[10] Garcia-Calderón G and Rubio A 1997 *Phys. Rev.* A **55** 3361.
[11] Garcia-Calderón G, Rubio A and Villavicencio J 1999 *Phys. Rev.* A **59** 1758.
[12] Romo R and Villavicencio J 1999 *Phys. Rev.* B **60** R2142.
[13] Moshinsky M 1952 *Phys. Rev.* **88**, 625.
[14] ——1976 *Am. J. Phys.* **44** (11) 1037.
[15] Steinberg A M, Kwait P G and Chiao R Y 1993 *Phys. Rev. Lett.* **71** 708.
[16] Chiao R Y 1993 *Phys. Rev.* A **48** R34.
[17] Enders A and Nimtz G 1993 *J. Phys. I France* **3** 1089.
[18] Nimtz G 1998 *Ann. Phys. (Leipzig)* **7** 618.
[19] Deutch J M and Low F E 1993 *Ann. Phys.*, NY. **228** 184.
[20] Note that the shutter is a device that aids to visualize the initial condition and hence it is not part of the system.

[21] The experimental observation of Sommerfeld and Brillouin precursors has already been reported in the microwave domain [Pleshko P and Palócz I 1969 *Phys. Rev. Lett.* **22** 1201].
[22] Krenzlin H M, Budczies J and Kehr K W 1998 *Ann. Phys. (Leipzig)* **7** 732.
[23] E. N. Dekanosidze, *Tables of Lommel's Functions of Two Variables* (Pergamon Press, New York, 1960) p. 1.
[24] M. Born and E. Wolf, *Principles of Optics* (Pergamon Press, Oxford, 1965) p. 438.
[25] Ranfagni A, Mugnai D and Agresti A 1991 *Phys. Lett. A* **158** 161.
[26] Jauho A P and Jonson M *Superlattices and Microstructures* 1989 **6** 303.
[27] Teranishi N, Kriman A M and Ferry D K *Superlattices and Microstructures* 1987 **3** 509.

Figure captions

Figure 1. Shutter problem for a potential step barrier V_0. An initial state $\psi(x,0)$ in the region $x<0$ is instantaneously released at $t=0$ by the removal of the shutter S.

Figure 2. Integration contours $C_2 = L+\Gamma_2+C_0+C_++C_-$ and $C_1 = L+\Gamma_1$, used to evaluate Eq. (7). The infinite semicircles Γ_1 and Γ_2 (dashed line) correspond to the cases $x>ct$ and $x<ct$, respectively.

Figure 3. The birth of $|\psi_r^s(x,t)|^2$ (solid line) as a function of distance x for increasing values of time: $t_1 = 0.001\ fs$, $t_2 = 0.0035\ fs$ and $t_3 = 0.0075\ fs$. Note that $|\psi_r^s(x,t)|^2$ fluctuates around the stationary solution $|\phi_r^s(x,t)|^2$ (dashed line). The inset shows at a later time $t_4 = 0.012\ fs$ the birth of a Sommerfeld-type precursor near the relativistic cutoff at $x = 3.0\ nm$.

Figure 4. Plot of $|\psi_r^s(x,t)|^2$ (solid line) as a function of distance x for a fixed value of time $t = 0.005\ fs$. Notice that the wave function exhibits a Sommerfeld-type precursor near the relativistic cutoff at $x = 15.0\ nm$. The precursor is accurately described in the vicinity of x=ct by a Bessel function (dotted line) given by equation (22). The stationary solution $|\phi_r^s(x,t)|^2$ (dashed line) is also depicted in the figure.

Figure 5. The main graph, as the previous one, shows the evolution of $|\psi_r^s(x,t)|^2$ (solid line) at a later time $t = 0.3\ fs$. Note that the main part of the wave reaches the stationary solution $|\phi_r^s(x,t)|^2$ (dashed line) at this short time. The small Sommerfeld-type precursor can be observed near the relativistic cutoff at $x = 90.0\ nm$. At the inset we show that the precursor (solid line), is well described by equation (22) (dotted line).

Figure 6. Time evolution of $|\psi_r^s(x,t)|^2$ for different values of the position: $x_1 = 0.4$ nm, $x_2 = 0.6\ nm$ and $x_3 = 0.8\ nm$. Notice that the transient behavior leading to the stationary regime exhibits an oscillating pattern similar to the *diffraction in time* phenomenon.

Figure 7. This graph illustrates $|\psi_r^s(x,t)|^2$ as a function of time for a fixed value of the position $x_1 = 3.0\ nm$, beyond $2x_p$. Notice that in this case, the diffraction-type pattern clearly disappears.

Figure 8. The time evolution of $|\psi_r^s(x,t)|^2$ in order to exhibit the main peak shift of the wave, for different values of the position: $x = 0.1\ nm$ (solid line), $x = 0.3\ nm$ (dashed line) and $x = 0.5\ nm$ (dotted line). The corresponding peak positions are p_3, p_2 and p_1, respectively. Despite the fact that the three curves fulfill relativistic causality, the wave front main peak exhibits an apparent violation of Einstein causality.

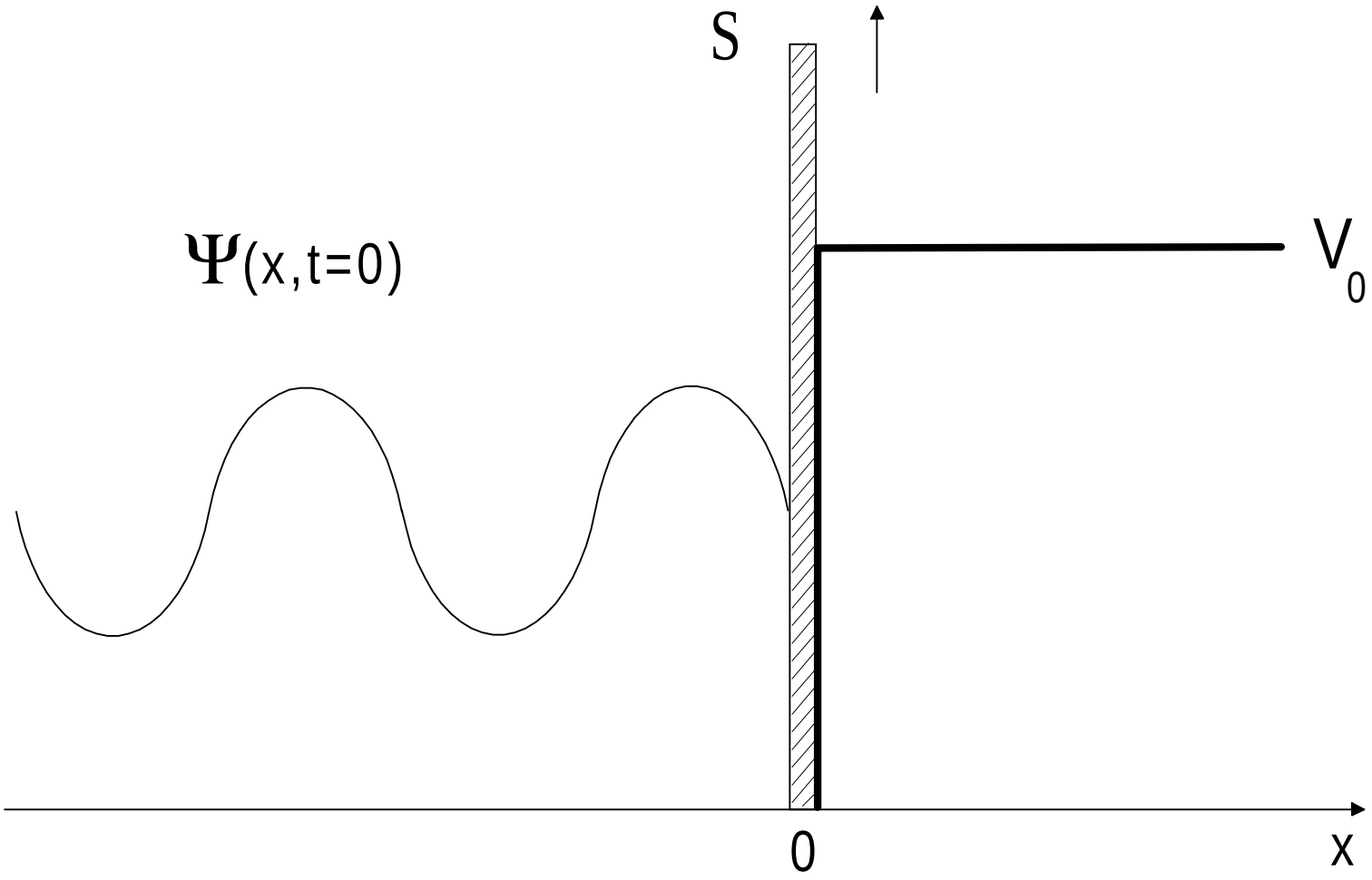

Fig. 1

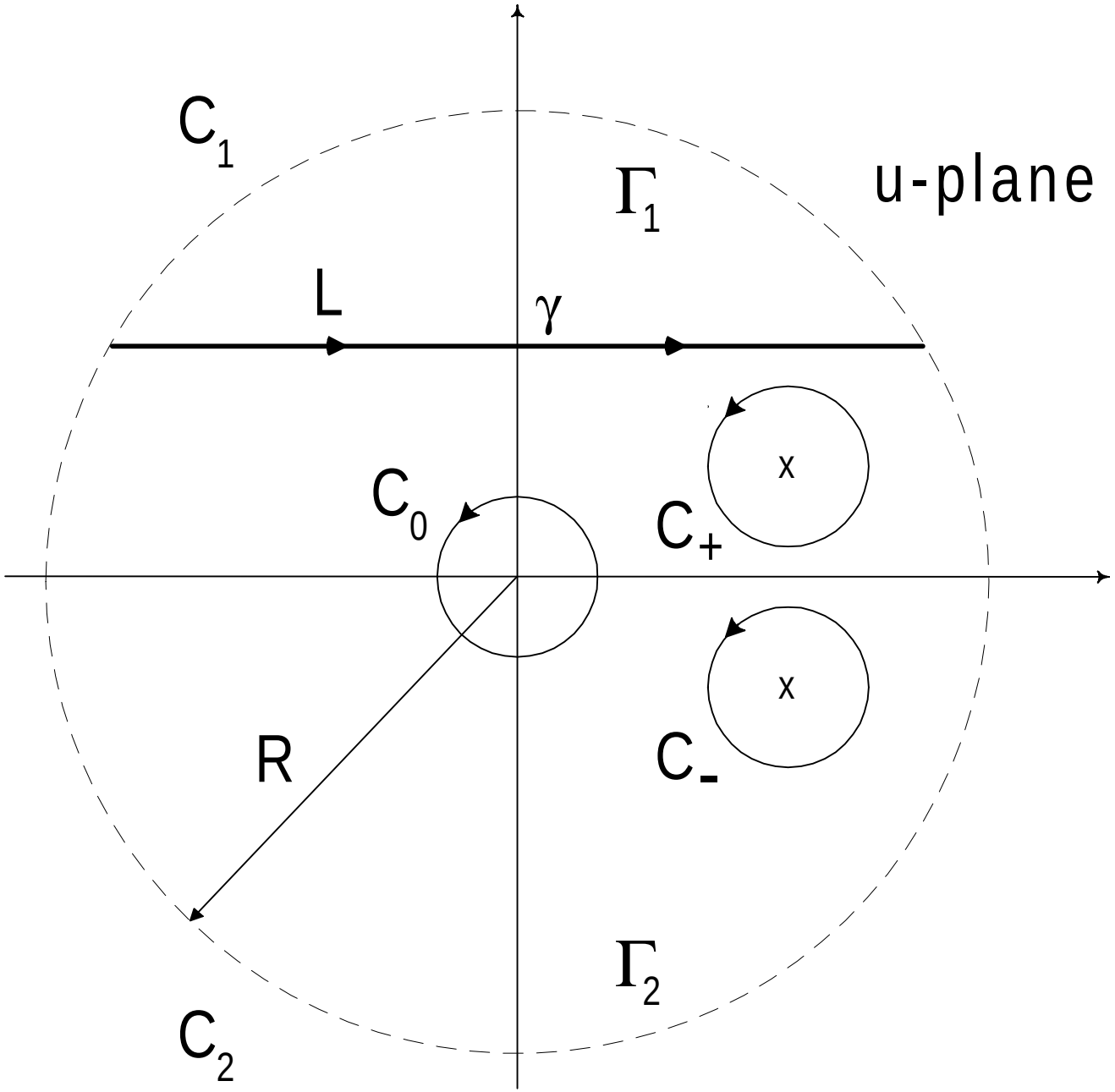

Fig. 2

Fig. 3

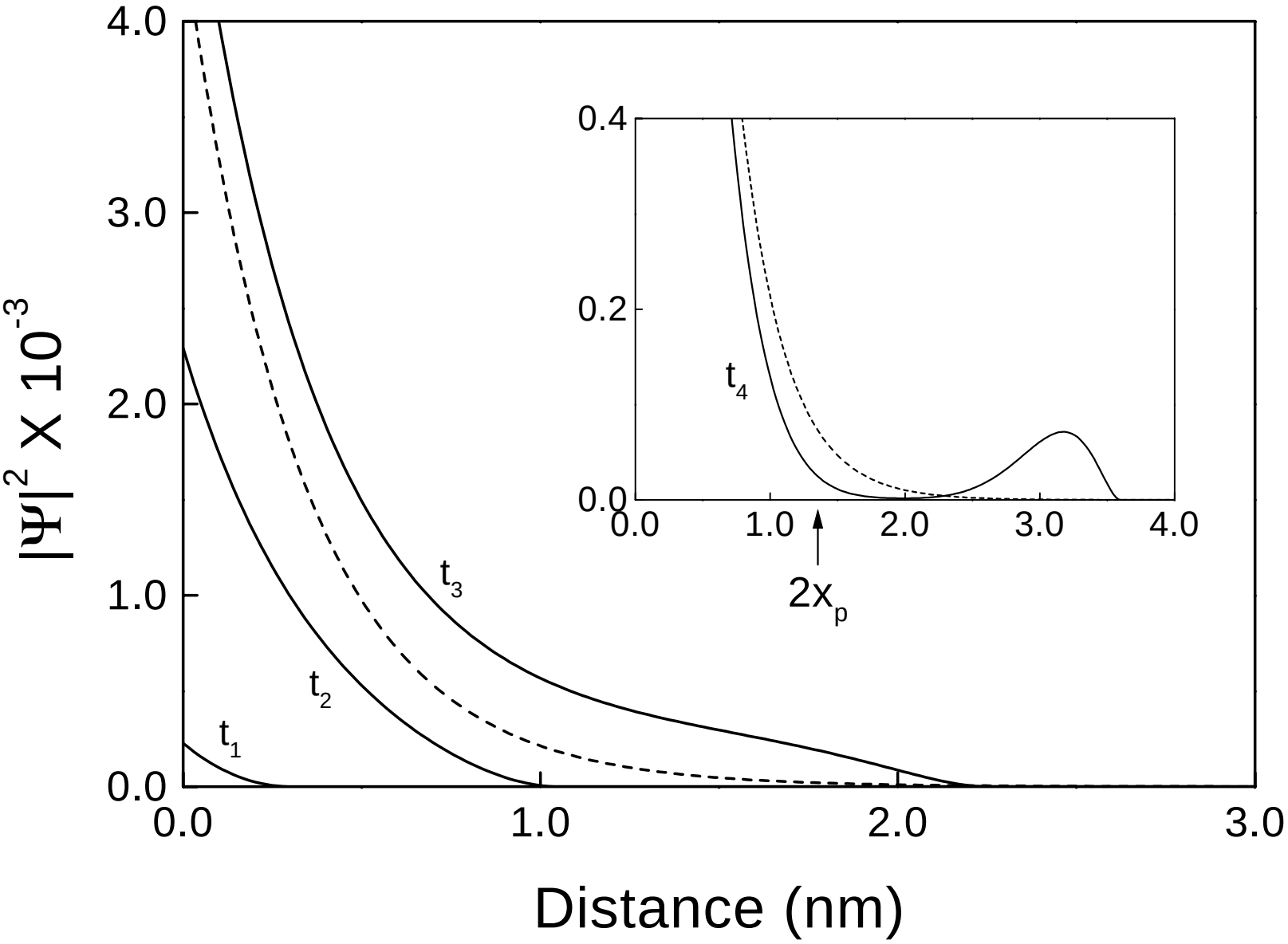
4.0
3.0
2.0
1.0
0.0
0.0
1.0
2.0
3.0
$|\Psi|^2$ X 10^{-3}
Distance (nm)
t_1
t_2
t_3
0.4
0.2
0.0
0.0
1.0
2.0
3.0
4.0
t_4
$2x_p$

Fig. 4

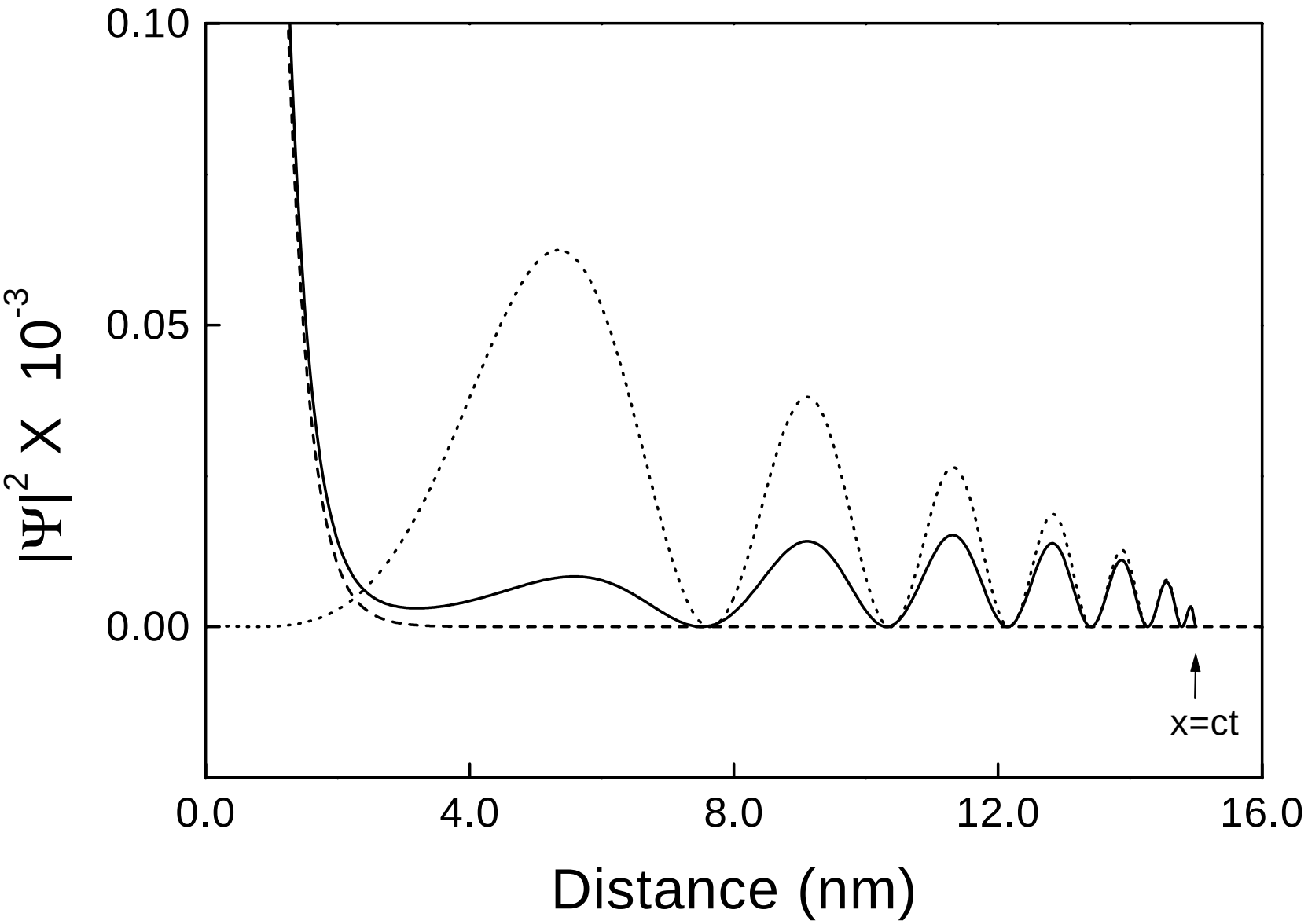

Fig. 5

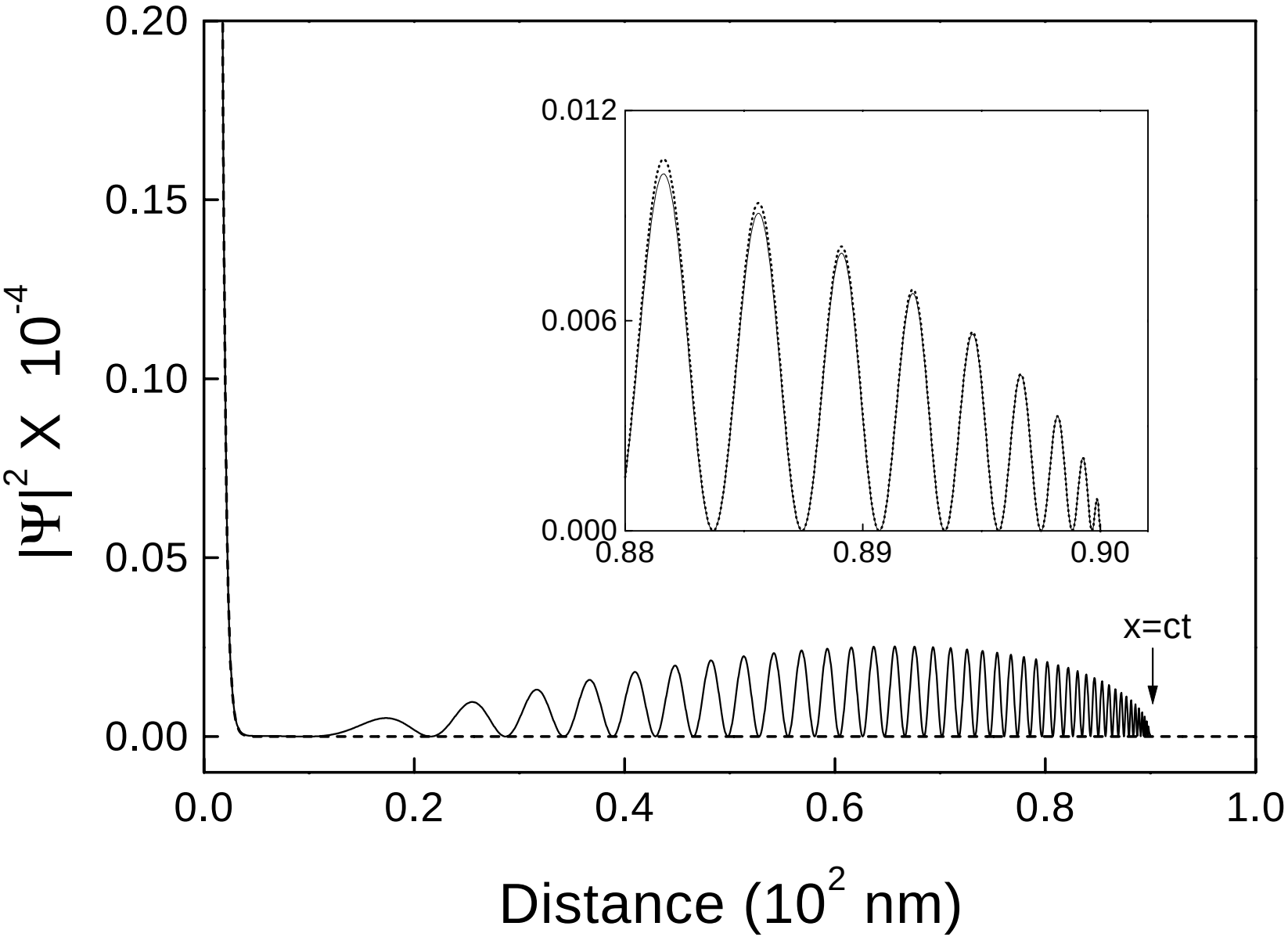
0.20
0.15
0.10
0.05
0.00
$|\Psi|^2$ X 10^{-4}
0.012
0.006
0.000
0.88
0.89
0.90
x=ct
0.0
0.2
0.4
0.6
0.8
1.0
Distance (10^2 nm)

Fig. 6

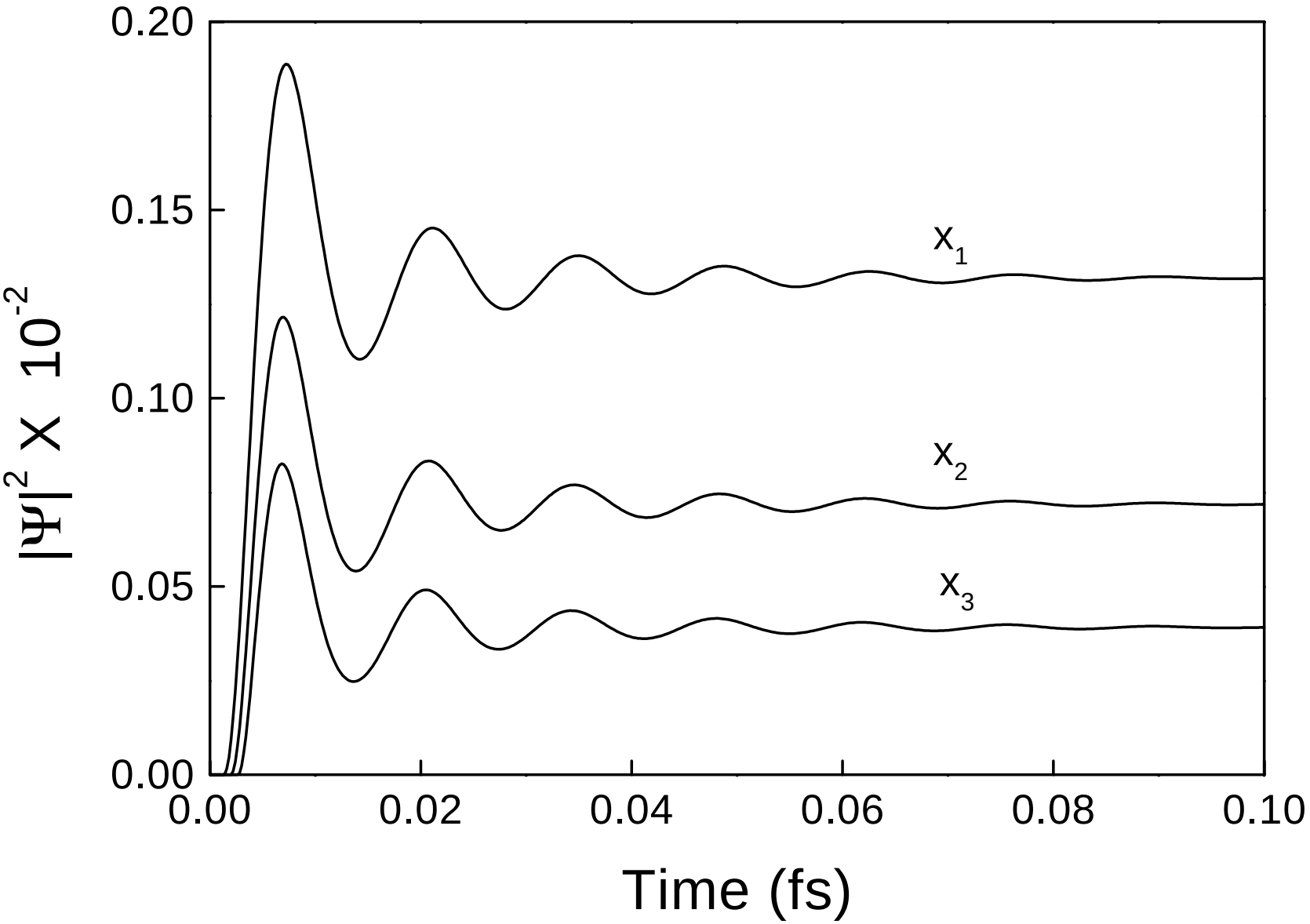
0.20
0.15
0.10
0.05
0.00
$|\Psi|^2$ X 10^{-2}
x_1
x_2
x_3
0.00
0.02
0.04
0.06
0.08
0.10
Time (fs)

Fig. 7

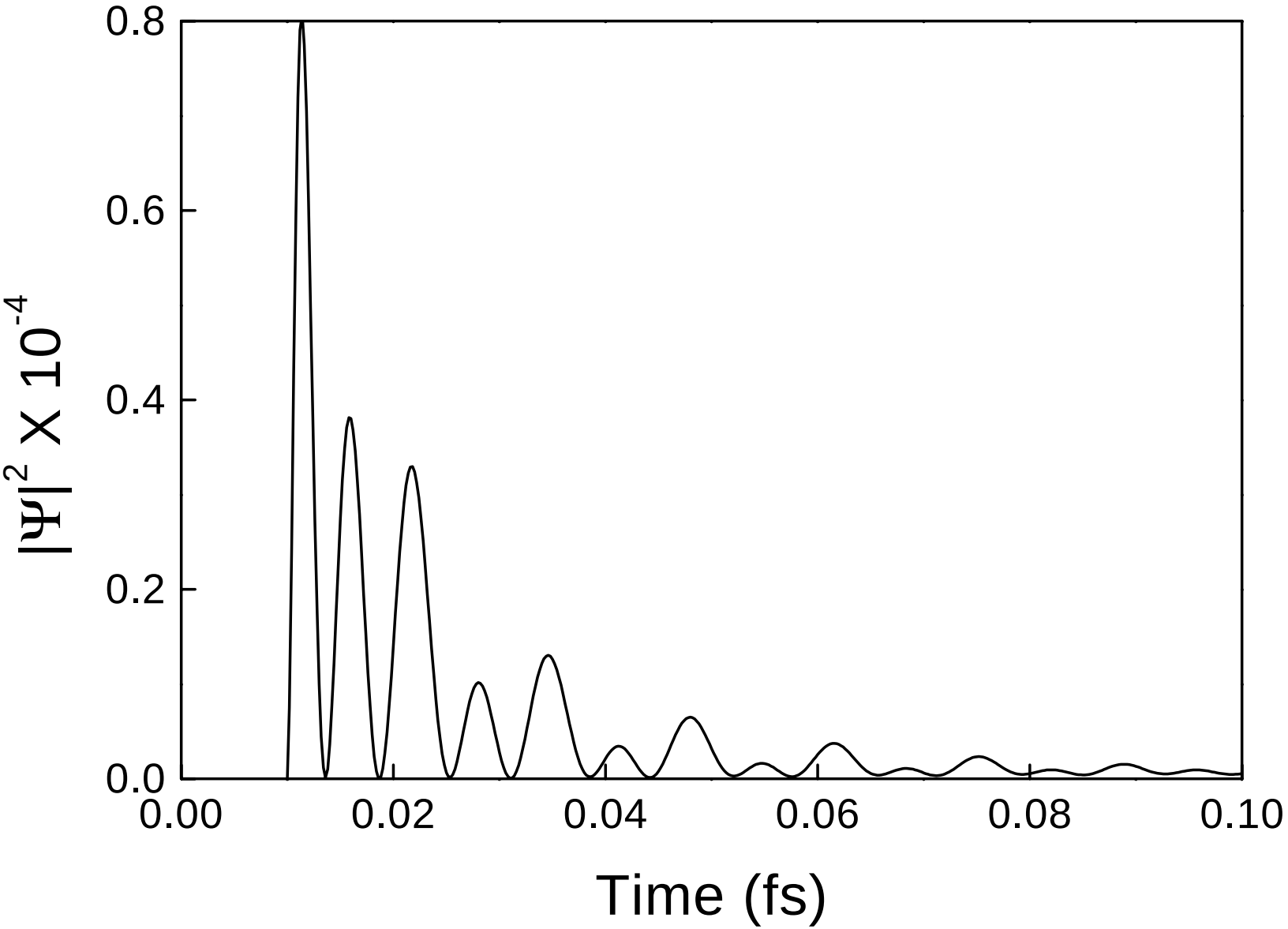

Fig. 8